Ultraviolet Photodissociation Dynamics of the 1-Methylallyl Radical

Michael Lucas^{a#}, Yuan Qin^{b#}, Lei Yang^b, Ge Sun^b, and Jingsong Zhang^{b*}

^a Department of Chemistry, University of Hawaii at Manoa, Honolulu, HI 96822, USA.

^b Department of Chemistry, University of California at Riverside, Riverside, CA 92521, USA.

* Corresponding author. E-mail: jingsong.zhang@ucr.edu. Fax: 1-951-827-4713. Also at the Air Pollution

Research Center, University of California, Riverside, CA 92521, USA.

M. L. and Y. Q. contributed equally to this paper.

Abstract

The ultraviolet (UV) photodissociation dynamics of the 1-methylallyl (1-MA) radical were studied using the high-n Rydberg atom time-of-flight (HRTOF) technique in the wavelength region of 226–244 nm. The 1-MA radicals were produced by 193-nm photodissociation of the 3-chloro-1-butene and 1-chloro-2-butene precursor. The 1+1 REMPI spectrum of 1-MA agrees with the previous UV absorption spectrum in this wavelength region. Quantum chemistry calculations show that the UV absorption is mainly attributed to the $3p_z$ Rydberg state (perpendicular to the allyl plane). The H-atom photofragment yield (PFY) spectrum of 1-MA from 3-chloro-1-butene displays a broad peak around 230 nm, while that from 1-chloro-2-butene peaks at ~ 236 nm. The translational energy distributions of the H-atom loss product channel, $P(E_T)$'s, show a bimodal distribution indicating two dissociation pathways in 1-MA. The major pathway is

isotropic in product angular distribution with $\beta \sim 0$ and has a low fraction of average translational energy in the total excess energy, $\langle f_{\rm T} \rangle$, in the range of 0.13-0.17; this pathway corresponds to unimolecular dissociation of 1-MA after internal conversion to form 1,3-butadiene + H. The minor pathway is anisotropic with $\beta \sim -0.23$ and has a large $\langle f_{\rm T} \rangle$ of ~ 0.62 -0.72. This fast pathway suggests a direct dissociation of the methyl H-atom on a repulsive excited state surface or on the repulsive part of the ground state surface to form 1,3-butadiene + H. The fast/slow pathway branching ratio is in the range of 0.03-0.08.

Keywords: 1-methylallyl radical, photodissociation, reaction dynamics, spectroscopy, electronically excited state.

Introduction

Resonance stabilized radicals (RSR) are of wide-ranging scientific importance, due to their stability from the delocalization of unpaired electrons throughout the framework. The allyl radical (C_3H_7) is the simplest and most studied RSR, with three unpaired π electrons delocalized over three carbon atoms. Methyl substitution of the allyl radical creates two C_4H_7 isomers, 1-methylallyl (1-MA) and 2-methylallyl (2-MA) radicals, the interest of which has increased recently. Similar to allyl, methylallyl radicals can be found in interstellar media as well as combustion processes, such as those of unsaturated fatty acid esters with C=C double bonds in biodiesel.

The focus of this work is the 1-MA radical, for which spectroscopic investigations have been reported through various techniques, including absorption, lelectron spin resonance, infrared, hotolegament, resonance-enhanced multiphoton ionization (REMPI), resonance Raman, and photofragment, spectroscopy. Callear and Lee reported a broad absorption spectrum of the 1-MA radical in the wavelength region of 226–238 nm, with the observation of several diffuse bands and the 0-0 band at 238 nm. Hudgens and coworkers measured the 2 + 1 REMPI spectra of *cis*- and *trans*-1-MA radicals between 455 nm and 485 nm. The observed absorption features were attributed to the intermediate state, $3p^2B_1$ Rydberg state. For the *trans*-1-MA, this excited state has a band origin of 237.7 nm and peaks at 236 nm, while for the *cis* 1-MA isomer, the band origin locates at 236.4 nm and the absorption peaks at \sim 232 nm. Gasser et al. measured the REMPI spectrum and the H-atom photofragmentation yield (PFY) spectrum of 1-MA at the \widetilde{A} \leftarrow \widetilde{X} transition in the wavelength range of 406 to 418 nm.

The energetics of the 1-methylally radical has been studied theoretically, ¹¹⁻¹⁷ and the H-loss dissociation pathways are shown in Figure 1. Miller studied the isomerization and dissociation of straight-chain C₄H₇ radicals. ¹³ Among the C₄H₇ isomers, *trans*-1-MA has the lowest energy.

The direct C-H bond fission of the methyl H from trans-1-MA radical to trans-1,3-butadiene + H has the lowest energy barrier of 45.3 kcal/mol. The lowest energy structural isomerization of trans-1-MA involves a 1,2-hydrogen shift from the methyl group that leads to trans-3-buten-1-yl with an energy barrier of 49.1 kcal/mol. Trans-1-MA can also undergo a 1,2-hydrogen shift from the allyl backbone and isomerize to the trans-2-buten-2-yl and trans-1-buten-2-yl radicals with barrier heights of 62.1 and 65.1 kcal/mol, respectively. A second pathway to the 1,3-butadiene + H products is via dissociation of the 3-buten-1-yl radical (with an overall barrier of 49.8 kcal/mol for the trans isomers). 1-MA can also dissociate to 1,2-butadiene + H through direct loss of the central allylic H-atom. After isomerizing from trans-1-MA, the isomer trans-1-buten-2-yl can undergo loss of the terminal β H-atom, resulting in the formation of 1-butyne + H. Additionally, after 1-MA isomerizes to 2-buten-2-yl, there are two H-loss pathways, the loss of a β H-atom to form 2butyne + H (substep barrier of 35.0 kcal/mol for the trans isomer) and the formation of 1,2butadiene + H from the C-H bond fission of the terminal β H-atom (substep barrier of 36.6 kcal/mol). The H-atom product channels and energetics for trans-1-MA from Figure 1 are summarized below.

trans-1-MA
$$\rightarrow$$
 trans-1,3-butadiene + H $\Delta H_{rxn,0} = 44.9 \text{ kcal/mol}$
 \rightarrow 1,2-butadiene + H $\Delta H_{rxn,0} = 56.8 \text{ kcal/mol}$
 \rightarrow 1-butyne + H $\Delta H_{rxn,0} = 57.9 \text{ kcal/mol}$
 \rightarrow 2-butyne + H $\Delta H_{rxn,0} = 52.6 \text{ kcal/mol}$

At 0.7 kcal/mol higher in energy than *trans*-1-MA (over a barrier of 14.0 kcal/mol), *cis*-1-MA has similar H-loss dissociation pathways except the 2-butyne + H channel. In addition to the H-atom

product channels mentioned above, there are also some methyl loss channels and an ethylene loss channel that can compete with the H-atom loss. The formation of allene + CH₃ can occur through a C–C bond fission of the *cis*-1-buten-2-yl isomer, featuring a transition state barrier \sim 5 kcal/mol lower than that for the production of 2-butyne + H. On the other hand, the generation of propyne + CH₃ from the *cis*-2-buten-2-yl isomer presents a barrier \sim 4 kcal/mol lower than that for the formation of 1,2-butadiene + H. Furthermore, the vinyl + ethylene products can be produced from both *trans*- and *cis*-3-buten-1-yl, with an overall energy barrier of \sim 53 kcal/mol with respective to *trans*- and *cis*-1-MA.¹¹

The H-atom loss channel in the photodissociation of 1-MA has been investigated by Gasser et al. in the range of 406 to 418 nm, where the first electronically excited state of 1-MA was characterized by the REMPI spectrum at the $\tilde{A} \leftarrow \tilde{X}$ transition. The time-dependent experiments revealed that the emergence of H atoms occurred on the nanosecond timescale, suggesting nonradiative decay to the ground state prior to H-atom loss in the ground state. A modest average product translational energy release of 8.6 kcal/mol was reported, consistent with statistical photodissociation of 1-MA to the product channel of 1,3-butadiene + H. The result of the photodissociation of 1-MA on the A-state is similar to the photodissociation dynamics of allyl from its Ã-state. The vibronic dynamics of the 1-MA excited state in the UV region of 232–237 nm was examined using resonance Raman spectroscopy by Tarrant and co-workers. ¹⁰ Significant excitation of the v17 and v18 carbon skeletal in-plane bending modes were observed, which could potentially precede bond dissociation, while the lack of intensity in the CH₃ stretches and the little intensity in the v16 C-CH₃ stretch suggest that the initial dynamics of the excited state does not proceed to the CH bond dissociation or rapid departure of the CH₃ group. Röder et al. examined this excited state of 1-MA in the broad UV absorption band of 226–238 nm using both electronic

structure calculations and time-resolved photoelectron spectroscopy.⁷ The time-dependent density-functional theory (TDDFT) and equation of motion coupled cluster with single and double excitations (EOM-CCSD) calculations indicated that this excited state has both 3p Rydberg and valence-excited $\pi\pi^*$ characters.⁷ The time-resolved photoelectron spectroscopy measurement of 1-MA at 238 nm and the time-resolved dynamics simulation showed a rapid decay of the excited state population (on the order of ~ 80 fs),⁷ indicating either rapid depopulation of the initially excited state to lower states, potentially via passage through a conical intersection, alteration in Franck-Condon (FC) factors as the wavepacket exits the observable range, or direct dissociation. So far, no reports have been made regarding the photodissociation dynamics or product distributions of 1-MA via the excited state at ~ 238 nm. In the present study, the UV photodissociation dynamics of the jet-cooled 1-MA radical in the UV photolysis region of 226-244 nm is explored using the high-n Rydberg time-of-flight (HRTOF) technique. In this study, the H-atom PFY spectra of the 1-methylally radicals were obtained, and the product translational energy and angular distributions of the H-atom loss channel were measured. Furthermore, this work reports the first observation of the non-statistical H-atom photodissociation dynamics of the 1-MA radical.

Experimental Methods

The HRTOF technique and experimental setup have been described in previous studies.¹⁸⁻²¹ The precursors used to generate the 1-MA radical were 1-chloro-2-butene (> 95%, Fisher Scientific) and 3-chloro-1-butene (97%, Sigma-Aldrich), which have been reported previously.¹, A pulsed 1-MA radical beam was produced by photolyzing a mixture containing ~ 2% of the precursor seeded in He (at a total pressure of ~120 kPa), with 193-nm radiation from an ArF

excimer laser. The generated 1-MA radicals were cooled by superionic expansion, and confirmed by vacuum ultraviolet (VUV) photoionization TOF mass spectrometry at 121.6 nm. The radical beam was crossed with a slightly focused UV photolysis laser radiation (at 226–244 nm, 0.25–1.5 mJ/pulse, linewidth 0.3 cm⁻¹), which photodissociated the 1-MA radicals. The polarization of the photolysis radiation was adjusted by rotating a Fresnel-Rhomb achromatic $\lambda/2$ plate for the Hatom product angular distribution measurements. The H atoms produced from the photodissociation of 1-MA were tagged through two-color resonant excitation, i.e. from 1²S to 2²P via the H-atom Lyman-α transition at 121.6 nm and subsequently further to a high-n Rydberg state by UV radiation at 366.3 nm. A small fraction of the metastable Rydberg H atoms drifted with their nascent velocities in the direction toward a microchannel plate detector that situated perpendicular to the molecular beam, and were field-ionized in front of the detector before being detected. The nominal flight length was calibrated to be 37.2 cm, using the 236 nm photodissociation of HBr with well-known dissociation energy and splitting energy of the $Br(^{2}P_{3/2})$ and $Br(^{2}P_{1/2})$ products. The ion signals were amplified through a fast preamplifier, and the H-atom TOF spectra were recorded and averaged by using a multichannel scaler. The number of laser shots of the TOF spectra varied, ranging from 100 to 500 k. The REMPI spectrum of 1-MA was obtained in the 233–240 nm region through a 1 + 1 ionization scheme using the HRTOF instrument in the TOF mass spectrometry mode. The signals of m/z = 55 ions were recorded as the UV laser wavelength scanned, and a Boxcar averager was employed to generate the REMPI spectrum of 1-MA.

Theoretical Methods

To supplement the earlier theoretical calculations,⁷ we explored the electronic transitions from ground state to the excited states of *trans*-1-MA and *cis*-1-MA using various quantum

chemistry methods. Ground state structures of the *trans/cis*-isomers were optimized using CCSD/aug-cc-pVDZ. The vertical excitation energies from the ground state to the lowest six excited states were then calculated with time-dependent DFT (TDDFT) (CAM-B3LYP) and EOM-CCSD methods under different basis sets (such as d-aug-cc-pVXZ, X=D, T, Q).²² The structures of the excited states with the highest oscillator strength were optimized using both TDDFT and EOM-CCSD. The adiabatic excitation energies were obtained from the difference between the electronic energy of the excited state and the ground state. To provide qualitative and illustrative interpretation of the electronic excitations, the natural transition orbitals (NTOs)²³ were analyzed under CAM-B3LYP/6-31++G. All the ab initio calculations in this work were performed with Gaussian 16, with the optimized geometries, excitation energies, transition dipole moments and NTO analysis results listed in the Supplementary Information (Table S1-S8 and Figure S1-S2).

Results

The TOF spectra of the H-atom products from the photodissociation of 1-MA were measured in the photolysis wavelength region of 226–244 nm. The measurements were conducted with the photolysis laser polarization oriented both parallel and perpendicular to the flight path. Various background TOF spectra were examined and removed to identify the correct H-atom signal from the 1-MA radical photodissociation, following the procedures described in previous studies. ^{18, 21, 24-25} The main background was attributed to the H-atom products from photodissociation of the 1-MA precursors. Figure 2 shows the net H-atom TOF spectra of 1-MA from the 1-chloro-2-butene and 3-chloro-1-butene precursors at 234 nm. Both TOF spectra show two distinct peaks, one prominently appearing at 35 μs and a smaller one at 18 μs. Specifically, the TOF spectrum obtained from 1-chloro-2-butene shows a more pronounced peak at 18 μs

compared to the spectrum derived from 3-chloro-1-butene. The resemblance between the two spectra suggests that the H-atom signal originated from a common source, the 1-MA radical. Figure 3 illustrates the H-atom TOF spectra obtained from 1-chloro-2-butene and the photolysis laser power dependence at 234 nm. Both the main peak at ~35 μs and the minor peak at ~18 μs exhibit a linear relationship with the photolysis laser power in the range of 0.4-1.2 mJ/pulse. The observed linear power dependence is consistent with a one-photon photodissociation process for both H-atom product channels.

To examine the electronic excited states of 1-MA involved in the photodissociation in the 226–244 nm region, two types of spectra were obtained: 1 + 1 REMPI spectrum (with the 3-chloro-1-butene precursor) and H-atom PFY spectra from the integrated HRTOF intensities (using both 3-chloro-1-butene and 1-chloro-2-butene precursors). Based on the conformational structures and previous UV photolysis studies of the two precursors, 10, 26-27 trans-1-MA should be the primary product from photolysis of 1-chloro-2-butene (in the lowest energy trans configuration), while photolysis of 3-chloro-1-butene would lead to both cis- and trans-1-MA. The 1-MA radicals were produced with low internal energy from the 193-nm photolysis of the precursors²⁶ and were further cooled in the molecular beam. The conformations of 1-MA, once produced in the photolysis of the precursors, were therefore preserved by the rigidity of the extended π bonding in the allylic moiety. 10 The 1-MA 1 + 1 REMPI spectrum in the 41700-42900 cm⁻¹ (233-240 nm) region is depicted in Figure 4(a). This spectrum exhibits five peaks at 42102, 42393, 42574, 42800, and 42912 cm⁻¹, in general agreement with the absorption spectrum (also with the 3-chloro-1-butene precursor) by Callear and Lee (Figure 4(a)). This confirms the production of 1-MA radicals in the molecular beam. Additionally, the peaks at 42393, 42574, and 42912 cm⁻¹ were previously identified as the excited electronic state with v18 H₃C-C-CC symmetric bend, v17 C-C-C

symmetric bend, and v16 C-CH₃ symmetric stretch, respectively. ¹⁰ Furthermore, the features between 233–238 nm in the REMPI spectrum in this work are similar to those in the 2 + 1 REMPI spectrum of *trans*-1-MA by Tsai et al.⁸ (Figure 4(b)). When comparing the 1 + 1 REMPI spectrum in this study with the 2 + 1 REMPI spectra of the trans and cis conformers by Tsai et al. (Figure 4(b), 8 it suggests that the composition of the 1-MA radicals from the photolysis of 3-chloro-1butene in this work had significantly more trans-1-MA than cis-1-MA. The H-atom PFY spectra (i.e. action spectra) for the 1-MA radicals (using both precursors) in the UV photolysis wavelength region of 226–244 nm are shown in Figure 4(c). The spectra were obtained by integrating the net H-atom TOF spectra as a function of photolysis wavelength in this region. To address the possibility of experimental condition fluctuations, the H-atom signals from 234 nm photolysis were monitored as a reference after every 3 to 4 measurements at other photolysis wavelengths. Subsequently, the H-atom intensities of all photolysis wavelengths were normalized to that of 234 nm and also with the photolysis laser power, and these two spectra were then scaled to their maxima, respectively. Both action spectra display a broad feature in this region. Specifically, the PFY spectrum derived from 3-chloro-1-butene displays a peak at 230 nm, whereas the PFY spectrum from 1-chloro-2-butene (which produces mainly *trans* 1-MA) shows a peak at 236 nm, consistent with the shape observed in the 2 + 1 REMPI spectrum of trans-1-MA. The variation between the two action spectra could result from the presence of different conformers of 1-MA produced from the two precursors.

To supplement our experimental findings, the excited electronic states of *trans*- and *cis*-1-MA were investigated using two quantum chemical methods: TDDFT and EOM-CCSD. Comprehensive calculation results are detailed in the Supplementary Information, including the structures of the *trans*- and *cis*-isomers, excited state energies, and transition dipole moments

(Table S1-S8 and Figure S1-S2). The excited energies of the six excited states (D_1 – D_6) have been computed for both trans- and cis-1-MA, and the calculations suggest that the UV excitation observed in the experiments in the region of 226-244 nm can be attributed to the fifth excited state (D₅) (for its similar electronic excitation energy and its largest oscillator strength), in agreement with the previous calculations by Röder et al.⁷ Among the methods and basis sets that give the above predictions, such as CAM-B3LYP/d-aug-cc-pVDZ, CAM-B3LYP/aug-cc-pVDZ, and EOM-CCSD/d-aug-cc-pVDZ, EOM-CCSD/d-aug-cc-pVDZ calculates the vertical and adiabatic energy of the excited D_5 state to be 234 nm and 238.5 nm for trans-1-MA (Table S3), respectively, overall in the closest agreements (especially for the adiabatic excitation energy) with the literature UV absorption spectrum, our 1 + 1 REMPI spectrum, and the previous 2 + 1 REMPI spectra. The dAug-cc-pVXZ augments include 2 shells of each angular momentum instead of one in Aug-ccpVXZ, making it more accurate for Rydberg excited states. Compared to trans-1-MA, the excitation energy from the ground state to D₅ is predicted to be higher for cis-1-MA (Tables S3 and S7), which is consistent with the 2 + 1 REMPI spectra of trans- and cis-1-MA by Tsai et al.⁸ Analysis on Natural Transition Orbitals (NTOs) reveals that the D₅ state has a dominant 3p Rydberg character and some $\pi \rightarrow n$ contribution (Table S4 and S8), with the involved Rydberg orbital perpendicular to the allyl plane, consistent with the previous calculations on the excited states of 1-MA by Röder et al. For both trans- and cis-1-MA, the computed transition dipole moment from the ground state to D₅ lies within the allyl plane (Table S4 and S8; Figure S1-S2). The higher energy state, D₆, exhibits comparable oscillator strength when excited from the ground state. However, it is less likely to be accessed in our experiments, as its energy is much beyond the wavelength region covered in this study.

The net H-atom TOF spectra of the jet-cooled 1-MA photodissociation are transformed to the product center-of-mass (CM) translational energy distribution, denoted as $P(E_T)$'s. The CM translational energy of the products, E_T , is converted from the H-atom flight time, t_H , using the following equation,

$$E_{\rm T} = \left(1 + \frac{m_{\rm H}}{m_{\rm C_A H_6}}\right) E_{\rm H} = \frac{1}{2} m_{\rm H} \left(1 + \frac{m_{\rm H}}{m_{\rm C_A H_6}}\right) \left(\frac{L}{t_{\rm H}}\right)^2 \tag{1}$$

where $E_{\rm H}$ represents the laboratory translational energies of the H-atom photofragment and L is the length of the TOF path. The $P(E_{\rm T})$ distribution from the 230 nm photodissociation of 1-MA at the two polarization angles, parallel ($\theta=0^{\circ}$) and perpendicular ($\theta=90^{\circ}$), i.e. $P_{\parallel}(E_{\rm T})$ and $P_{\perp}(E_{\rm T})$, are illustrated by solid black lines in Figure 5(a) and 5(c). The product CM translational energy and photofragment angular distribution are described by the following equation: $P(E_{\rm T},\theta)=\frac{1}{4\pi}P(E_T)[1+\beta P_2(cos\theta)]$, where θ is the angle between the recoiling velocity of the H-atom product and the electric vector of the linearly polarized photolysis radiation, $P(E_{\rm T})$ is the angle-integrated product translational energy distribution, β is the anisotropy parameter ($-1 \le \beta \le 2$), and $P_2(cos\theta)$ represents the second Legendre polynomial. The $E_{\rm T}$ dependent anisotropy parameter, $\beta(E_{\rm T})$, can be derived with $\beta(E_{\rm T}) = \frac{2[P_{\parallel}(E_T) - P_{\perp}(E_T)]}{P_{\parallel}(E_T) + 2P_{\perp}(E_T)}$, which is displayed in Figure 5(d). At the magic angle $\theta=54.7^{\circ}$, $P_m(E_{\rm T})$ is independent of β and can be calculated from $P_{\parallel}(E_{\rm T})$ and $P_{\perp}(E_{\rm T})$, as shown in Figure 5(b). Given $P_m(E_{\rm T}) = (1/4\pi)P(E_{\rm T})$, $P_m(E_{\rm T})$ is utilized to evaluate the translational energy release and the product branching ratios.

The $P(E_T)$ distributions at the three different polarizations in Figure 5 exhibit a bimodal distribution. The primary channel exhibits a peak at a lower translational energy of ~ 7 kcal/mol, while the minor channel displays a peak at a higher translational energy of ~ 50 kcal/mol and

extends to the maximum available energy for the 1,3-butadiene + H product channel (79.4 kcal/mol). Figure 5 also indicates the maximum available energy for the other H-atom product channels, specifically 67.5 kcal/mol for 1,2-butadiene + H and 66.4 kcal/mol for 1-butyne + H. The maximum available energy is the difference between the photolysis photon energy and the dissociation energy of the channel (assuming the internal energies of the radicals and the photodissociation fragments are ~ 0). The dominant component of the $P(E_T)$ distribution below 35 kcal/mol is similar at different polarizations, which indicates an isotropic angular distribution ($\beta \approx$ 0). The minor component ($E_T > 40$ kcal/mol) exhibits higher intensity when the polarization is perpendicular compared to parallel. The β value is ~ -0.23 for the minor component, indicating an anisotropic angular distribution. The different β values suggest that there are at least two dissociation channels. To isolate the contributions from these dissociation pathways, the observed $P(E_{\rm T})$ and $\beta(E_{\rm T})$ can be expressed as follows: $P(E_{\rm T}) = P_{\rm I}(E_{\rm T}) + P_{\rm II}(E_{\rm T})$ and $\beta(E_{\rm T}) =$ $x_{\rm I}(E_{\rm T})\beta_{\rm I} + x_{\rm II}(E_{\rm T})\beta_{\rm II}$, where $P_i(E_{\rm T})$ and β_i correspond to the respective ith channel, and $x_i =$ $P_i(E_T)/P(E_T)$ represents the energy-dependent branching fraction of the ith channel. 49 Assuming that the β value remains a constant ~ 0 for the slow component and $\beta \approx -0.23$ for the fast one, the $P_m(E_T)$ distribution is deconvoluted into a fast (I) and a slow (II) component (as shown in Figure 5(b)).

Based on the deconvolution, the average translational energy release, $\langle E_T \rangle$, and the fraction of the average translational energy release in the total available energy, $\langle f_T \rangle$, can be calculated for each component. Assuming the lowest energy pathway to the 1,3-butadiene + H products (discussed later), at 230 nm, $\langle E_T \rangle$ of the fast channel (I) is ~ 51 kcal/mol with $\langle f_T \rangle \approx 0.64$. For the slow channel (II), $\langle E_T \rangle \approx 11$ kcal/mol with $\langle f_T \rangle \approx 0.14$ when using the 3-chloro-1-butene precursor, and $\langle E_T \rangle \approx 12$ kcal/mol with $\langle f_T \rangle \approx 0.15$ for the 1-chloro-2-butene precursor,

respectively. The overall $\langle f_{\rm T} \rangle$ value of the H-loss product channel at 230 nm is ~ 0.15 for the 3chloro-1-butene precursor and ~ 0.18 for the 1-chloro-2-butene precursor, showing a modest amount of overall translational energy release. Examining the $P(E_T)$ distributions at other photolysis wavelengths from 226 to 244 nm reveals a range of $\langle f_{\rm T} \rangle$ values as depicted in Figure 6. With the 3-chloro-1-butene precursor, the $\langle f_{\rm T} \rangle$ of the slow channel ranges from 0.13 to 0.15, averaging around 0.15, while for the 1-chloro-2-butene precursors, the slow channel (II) exhibits a slightly larger $\langle f_T \rangle$ of ~ 0.16. On the other hand, the fast product channel (I), for both the 3-chloro-1-butene and 1-chloro-2-butene precursor, displays a substantial $\langle f_{\rm T} \rangle$ ranging from 0.62 to 0.72 (with an average ~ 0.67). At 230 nm, the integration of the fitted components I and II from the $P_{\rm m}(E_{\rm T})$ distribution in Figure 5 (derived from the 1-chloro-2-butene precursor) estimates a branching ratio of the fast to slow components at ~ 0.07 . Similarly, the branching ratios of the fast to slow components at the photolysis wavelengths range of 226-244 nm are estimated and summarized in Figure 7. For the 3-chloro-1-butene precursor, the branching ratio values fluctuate within the range of 0.03 to 0.06, averaging \sim 0.04. Conversely, the 1-chloro-2-butene precursor yields larger branching ratios, ranging from 0.06 to 0.08 with an average of 0.07. These values do not show a clear trend, possibly due to the relatively low intensity of the fast component in the data.

The H-atom yield time profile in the UV photolysis of 1-MA was investigated as a function of the time delay between the photolysis and probe lasers. The time profile in Figure 8 was obtained by integrating the HRTOF spectra at 230 nm with different photolysis-probe delay times, which provides the measurement of the microcanonical rate of the unimolecular dissociation of 1-MA. The initial rise of the signal gives the rate of the H-atom formation from 1-MA, while the decay of the signal after the peak is attributed to the H-atom flight out of the interaction region between

the photolysis and probe lasers. To estimate the unimolecular dissociation rate of 1-MA, the time profile of the H-atom signals, $S_{\rm H}(t)$, is fitted using an equation based on the previous work from Chen's group:²⁸

$$S_{\rm H}(t) = N[1 - \exp(-k_{\rm H}t)] \cdot \left[\frac{1}{\exp[(t-a)/b] + 1}\right]$$
 (2)

where $k_{\rm H}$ represents the unimolecular dissociation rate constant for the H-atom formation from the 1-MA radical, and a and b are constants that characterize the width of the plateau region and the decay of the signal. The fitting is shown as the solid line in Figure 8, giving a dissociation rate constant $k_{\rm H} \sim 1.9 \times 10^8 \; {\rm s}^{-1}$ at 230 nm. As the H-atom signal monotonically decays after 10 ns, which is limited by the 10-ns time resolution of the pump and probe laser radiation, this $k_{\rm H}$ value is reported as the lower limit of the actual dissociation rate constant. The decay of the H-atom signal after the peak is also simulated based on the H-atom translational energy distribution and the size of the laser interaction region and is confirmed to be due to the H-atom flight out of the laser interaction region (see Figure S6 in Supplementary Information).

Discussion

The UV photodissociation of the jet-cooled 1-MA radical was investigated in the range of 226–244 nm for the first time. This study explores the C₄H₆ + H photodissociation channels by measuring the H-atom product TOF spectra. The good agreement of the two TOF spectra from the two different precursors in Figure 2 shows that the H-atom signal arises from the same species, further supporting the production of the 1-MA radical. Compared to the H-atom TOF spectrum derived from the 3-chloro-1-butene precursor, the 1-MA derived from 1-chloro-2-butene exhibits a more pronounced peak for its fast component in the H-atom TOF spectrum. The action spectra

of 1-MA in the region 226–244 nm from both precursors show a broad feature (Figure 4(c)). The one from the 1-chloro-2-butene precursor (which produced mostly the *trans*-1-MA) is in good agreement with the 2 + 1 REMPI spectrum of *trans*-1-MA by Tsai et al,⁸ and that from 3-chloro-1-butene (which produced both *trans*- and *cis*-1-MA) shifts to shorter wavelengths, and does not match the absorption spectrum by Callear and Lee that peaks at 237.8 nm¹ or our 1 + 1 REMPI spectrum (both using the 3-chloro-1-butene precursor). As shown in our electronic structure calculations and the 2 + 1 REMPI spectra of *trans*- and *cis*-1-MA by Tsai et al,⁸ the D₅ state in *cis*-1-MA has a higher excitation energy compared to that in *trans*-1-MA. The difference between these spectra using the 3-chloro-1-butene precursor is possibly due to a higher production of *cis*-1-MA from the photolysis of 3-chloro-1-butene under the specific experimental conditions during the PFY spectra measurements or that *cis*-1-MA has a higher H-atom yield than *trans*-1-MA.

The CM translational energy distributions of the H-atom product channel in the region of 226–244 nm are similar to each other. As illustrated in Figure 5 for the case of 230 nm, the $P(E_T)$ distributions as well as the angular distribution of the H-atom product exhibit a bimodal pattern, unlike the previous ones of 1-MA via the \tilde{A} state at lower excitation energy⁹ and those in the UV photodissociation of allyl,²⁵ which only exhibited a low-energy feature. The larger (slow) peak is centered at ~ 7 kcal/mol and extends up to ~ 50 kcal/mol, with a modest $\langle f_T \rangle$ of ~ 0.15 in the photolysis wavelength region of 226–244 nm (Figure 6). This broad, low energy peak feature of the $P(E_T)$ suggests a statistical-like product energy distribution in the unimolecular dissociation of a molecule. The slow component (II) shows an isotropic angular distribution ($\beta \approx 0$), indicating that the dissociation timescale is longer than the rotational period of the 1-MA radical, exceeding the ps range. This timescale is consistent with the non-repulsive photodissociation process and supports the hot radical photodissociation mechanism where 1-MA dissociates on the vibrationally

excited ground electronic state after internal conversion from the excited D_5 (mainly the 3p Rydberg) state. The relaxation dynamics study on the excited states of 1-MA suggests that the initially excited D_5 state undergoes rapid decay to the lowest excited \tilde{A} state, which then subsequently deactivates to the electronic ground state within a picosecond time scale.⁷ The hot radical on the ground electronic state then takes an additional amount time to undergo unimolecular dissociation.

As the photon energy used for photodissociation (117.2–126.5 kcal/mol) is higher than the barriers of all the H-loss pathways of 1-MA, it is possible that all the H-atom product channels would make contributions to the slow component (II) (Figure 1). The lowest energy product channel is 1,3-butadiene + H ($\Delta H_{rxn,0}$ = 44.9 kcal/mol for trans-1-MA, and 47.2 kcal/mol for cis-1-MA). There are two pathways that lead to the formation of 1,3-butadiene + H, and both pathways are the lowest energy routes for 1-MA decomposition. The lower of these two pathways involves the direct release of an H-atom from the methyl group, requiring overcoming a barrier of 45.3 kcal/mol for trans-1-MA (47.4 kcal/mol for the cis radical). The alternative pathway entails a 1,2hydrogen shift to 3-buten-1-yl, subsequently leading to H-atom loss and the formation of 1,3butadiene. Besides the direct release of an H-atom from the methyl group, 1-MA can also undergo the direct loss of the central H-atom situated on the allyl backbone, leading to the formation of 1,2butadiene + H with $\Delta H_{rxn,0} = 56.8$ kcal/mol (for trans-1-MA). The other higher energy H-atom product channels involve a 1,2-hydrogen shift to 2-buten-2-yl (isomerization barrier = 62.1 kcal/mol), leading to subsequent H-atom loss and the formation of either 2-butyne + H or 1,2butadiene + H. Additionally, there is the possibility of 1-butyne + H formation following an isomerization to 1-buten-2-yl (barrier = 65.1 kcal/mol). Previous RRKM rate calculations for the ground state 1-MA radical at an internal energy of ~ 112 kcal/mol by Ribeiro and Mebel¹⁴ indicated that apart from the isomerization reaction between *trans*-1-MA and *cis*-1-MA (which is much faster), the direct dissociation to 1,3-butadiene + H predominates among other unimolecular reactions of 1-MA. Assuming *trans*- and *cis*-1-MA conversion reaches equilibrium, ~ 85% of the *trans*-1-MA radicals dissociate into *trans*-1,3-butadiene + H with a rate constant $k = 3.40 \times 10^{10}$ s⁻¹ ($k = 6.95 \times 10^9$ s⁻¹ for *cis*-1-MA). Our pump-probe delay experiment provided a lower limit on the rate constant for the product of H-atom of 1.9×10^8 s⁻¹ (Figure 8), which is consistent with the RRKM calculations.

As the slow component in the $P(E_T)$ exhibits a statistical distribution, it suggests that the most likely photodissociation channel is the lowest energy channel, which corresponds to the production of 1,3-butadiene + H. This agrees with previous findings by Gasser et al., 9 which also proposed a statistical distribution for dissociation of 1-MA via the A state. This implies a nonradiative transition of 1-MA from the electronically excited D₅ state to the ground electronic state, ⁷ followed by H-atom loss, resulting in the low-energy product channel of 1,3-butadiene + H. The average E_T of the slow component in Figure 5 is approximately 10.1 kcal/mol, which is similar to the previously reported value of 8.6 kcal/mol for the 1-MA A state by Gasser et al. However, the value of $\langle f_{\rm T} \rangle$ in Figure 6 is lower in this experiment compared to the previously reported value (0.15 vs. 0.36). This difference is anticipated due to the use of higher-energy photolysis photons (230 nm) in this study compared to the previous study (415 nm). The results obtained by Gasser et al. were comparable to those observed in the photodissociation of the allyl radical after photoexcitation to the à state.²⁹ This study also shares similarities with the photodissociation of the allyl radical in a similar photolysis wavelength range of 216–249 nm.²⁵ Song et al.²⁵ reported an average value of $\langle f_T \rangle$ in the range of 0.18–0.22 for allyl in the photolysis region spanning 216– 249 nm, which is similar to the 0.14–0.15 range observed for the slow component of $P(E_T)$ in the

case of 1-MA. The photodissociation mechanism of allyl follows a statistical process. The resemblance of the low-energy $P(E_T)$ feature in 1-MA to the previous photodissociation studies of 1-MA and allyl implies that this feature is also driven by a statistical mechanism, involving H-atom dissociation after internal conversion from the electronically excited state to the highly vibrationally excited ground electronic state. The primary product for this slow component is most likely 1,3-butadiene + H, although the other H-atom channels may also make contributions.

To simulate the translational energy distribution of the products of the slow component in the UV photodissociation of 1-MA, statistical prior distribution models of the product energy distribution $P(E_T)$ using ab initio reaction energetics are utilized here to calculate the partitions of internal and translational energies in the products. The optimized structures and relative energies of the species along the potential energy surface (PES) from trans-1-MA to trans-1,3-butadiene + H (at 44.6 kcal/mol), as well as the transition state (TS) (at 47.0 kcal/mol) are from calculations by Ribeiro and coworkers at CCSD(T)-F12/CBS//B3LYP/6-311G(d,p) + ZPE(B3LYP/6-311G(d,p)) level of theory, ¹⁴ which are utilized in our $P(E_T)$ calculations. The photon energy absorbed by trans-1-MA in the experiment is considered as the total available energy (E_{total}) of the highly internally excited ground-state trans-1-MA. In the dissociation process, E_{total} is distributed into the rovibrational energy of 1,3-butadiene ($E_{\rm VR}$) and the relative translational energy of the two departing fragments (E_T) . The rovibrational densities of states for 1,3-butadiene and the $P(E_T)$ distribution of the 1,3-butadiene + H products are calculated using the Mesmer coding package.³⁰ Three statistical models are utilized to estimate the nascent internal energy distribution of 1,3butadiene from the unimolecular dissociation of trans-1-MA.³¹ In the fully statistical (FS) model, all the available energy ($E_{\text{excess}} = E_{\text{total}} - E_{\text{products}}$) is assumed to be statistically distributed over E_{VR} and E_T , with rapid energy exchange between the fragments. The statistical-strong repulsion (SSR)

model assumes that only the energy above the dissociation barrier ($E_{\text{total}} - E_{\text{TS}}$) is statistically distributed, with the remaining energy, the energy of the exit channel barrier ($E_{TS} - E_{products}$), allocated entirely to the relative translational energy of the fragments. The statistical-trajectory potential (STP) model treats part of the exit channel barrier ($E_{TS} - E_{products}$) released as translational energy, with the rest of this energy, along the energy above the dissociation barrier ($E_{\text{total}} - E_{\text{TS}}$), distributed statistically over E_{VR} and E_{T} . The normalized rovibrational energy distributions of 1,3butadiene ($E_{\rm VR}$) calculated from the three statistical models at 230 nm are presented in Figure S3. The product translational energy distributions, $P(E_T)$'s, from the three statistical models are then derived by subtracting E_{VR} from E_{total} , as shown in Figure S4 and Figure 9. At the excitation energy of 230 nm, the $P(E_T)$ from the SSR model agrees with the experimental $P(E_T)$ of the slow component in the range of $E_T < \sim 5$ kcal/mol and at the peak position, while that from the STP model (assuming 50% of the energy of the exit channel barrier released in products' translation) peaks at a lower energy and that from the FS model further lower in energy. This trend shows the visible impact of the exit channel barrier on the $P(E_T)$ in the unimolecular dissociation. The SSR statistical prior distribution model, when compared with the experimental $P(E_T)$ of the slow component, is qualitatively consistent with the statistical unimolecular dissociation of trans-1-MA to 1,3-butadiene + H over a small exit barrier, but it underestimates the product translational energy release (i.e., predicting lower distribution at E_T in the region of ~ 10 to 30 kcal/mol). The same simulations are applied to the dissociation of trans-1-MA at 24080 cm⁻¹ (via the first electronically excited state as investigated by Gasser et al. 9), showing a similar trend in the $P(E_T)$ distribution of the 1,3-butadiene + H products (Figure S5). The derived average E_T from the SSR model, 5.3 kcal/mol, is closest among the three models to the experimental value of 8.6 kcal/mol by Gasser et al.9 It should be noted that the statistical prior distribution models used here are relatively simple

models for the $P(E_T)$ distribution, and they qualitatively describe the statistical unimolecular dissociation. However, they tend to underestimate the product translational energy release, and other statistical models may need to be explored for quantitive agreement.

Compared to the slow feature, the fast component (I) is small, and identification becomes challenging after transformation from the TOF spectra to the $P(E_T)$ distributions. The smaller (fast) component in the CM translational energy distribution is centered at ~ 50 kcal/mol and extends to ~ 80 kcal/mol, marking the appearance of the lowest energy product channel, 1,3-butadiene + H (Figure 5(a)-(c)). The $\langle f_{\rm T} \rangle$ for this feature is large in the range of 0.62–0.72 for the photolysis wavelength region studied (Figure 6). This high energy feature of the $P(E_T)$ is consistent with a non-statistical distribution. In Figure 5(d), the β value decreases from 0 to ~ -0.23 at ~ 50 kcal/mol and remains constant up to the threshold of the 1,3-butadiene + H product channel at 79.4 kcal/mol. The fast component, characterized by its anisotropy, indicates that the photodissociation process is repulsive and takes place more rapidly than the rotational period of the radical, prior to its reorientation. This agrees with the idea that the non-statistical feature in the $P(E_T)$ results from direct dissociation on an electronically excited state or a repulsive segment of the ground state, possibly facilitated by a conical intersection connecting the 3p Rydberg state, leading to the formation of 1,3-butadiene + H. The structural disparity between 1-MA and allyl lies in the terminal methyl group of 1-MA. Given that the previous study on the UV photodissociation of allyl did not exhibit a discernible high-energy feature, 25 it implies that instead of H loss from the allylic backbone, the fast component is likely attributed to the removal of an H-atom from the methyl group in 1-MA. This would result in the direct formation of the 1,3-butadiene + H product channel. The negative β value of the fast component (I) suggests that in a prompt dissociation the direction of the departing H atom is approximately perpendicular to the transition dipole moment

 μ between the ground \tilde{X} state (A") and the excited D₅ state. The measured β value of -0.23indicates a 60° angle between μ and the velocity direction of the departing H atom in the prompt dissociation. $^{32-33}$ The theoretical calculations show that the $3p_z$ character dominates in the excited D_5 states (A"), whose orbital is perpendicular to the allylic plane. Thus, the symmetry of μ is A', and it lies in the molecular plane based on our calculations utilizing the method of Röder et al.⁷ (Figure S1 and S2 and Table S4 and S8). This would result in a negative β parameter when a methyl H atom departs out of the carbon skeleton plane, leading to the prompt production of 1,3butadiene. Based on the calculated ground state geometry, upon the vertical electronic excitation, the angle between the direction of μ and the out-of-plane C-H bond on the CH₃ group is estimated to be $\sim 58^{\circ}$, whereas the angle between μ and the in-plane C–H bond on the CH₃ group is $\sim 95^{\circ}$. When using the optimized structure of the D₅ excited state, this angle is predicted to be 60° for the out-of-plane C-H bond and 91° for the in-plane C-H bond on the CH₃ group. Therefore, the experimentally deduced angle of 60° from the observed β value of -0.23 supports the conclusion that the prompt dissociation in the fast component (I) proceeds via the breaking of the out-of-plane C-H bond on the CH₃ group. The previous resonance Raman spectra conducted by Tarrant et al. ¹⁰ revealed notable features of excitation of 1-MA in the CCC in-plane bend and weak intensity in the C-CH₃ stretch, but no evidence of excitation in the CH stretch in the FC region on the excited state. This implies little or no C-H dissociation initiated in the FC region. However, this could still be consistent with our observation of the prompt, direct C–H dissociation in the fast component, as it is a minor channel and may not be readily discernible in the previous resonance Raman spectra.

Overall, the results of 1-MA are similar to those of its isomer, 2-MA, which also exhibits two distinct features in the production of the 1,3-butadiene + H products in the same photodissociation wavelength region. As observed in our recent work on the photodissociation of

2-MA via the 3p Rydberg state in 226–244 nm, the slow component is broad in $P(E_T)$ with a $\langle f_T \rangle$ of 0.16–0.19 and shows an isotropic angular distribution.³⁴ The fast component is a small peak at ~ 50 kcal/mol, with $\langle f_{\rm T} \rangle = 0.58 - 0.68$ and $\beta \sim -0.2$. The fast component of 2-MA is less conspicuous than that of 1-MA, having a smaller fast/slow branching ratio of $\sim 0.02-0.03$. The higher contribution of the fast component in 1-MA (fast/slow ratio $\sim 0.03-0.08$) may be attributed to the more straightforward direct H-loss pathway to 1,3-butadiene + H, whereas 2-MA must undergo isomerization before releasing an H atom to produce 1,3-butadiene + H. It can be concluded that the outcomes of the overall photodissociation are determined by the energetics and isomerization pathways involved. Based on our theoretical calculations and those by Röder et al.⁷, the UV excitation of 1-MA in this study is attributed to the fifth excited state D₅ with dominant 3p Rydberg character. The involved Rydberg orbital is predicted to be perpendicular to the allyl plane, analogous to what was established for allyl and 2-MA. For 2-MA, we proposed that the fast component comes from a minor isomerization process to form 1-MA on the excited surfaces, followed by a rapid, direct, and repulsive loss of H and production of 1,3-butadiene + H. The similar observations of the fast component in 1-MA, but with a higher contribution than in 2-MA, support this speculation and is consistent with the fact that 1-MA can directly produce 1,3butadiene + H without any isomerization.

Conclusions

The UV photodissociation of jet-cooled 1-MA was analyzed with a focus on the H-atom product channels in the range of 226 nm to 244 nm via the $3p_z$ Rydberg state. The H-atom product translational energy release and angular distribution have a bimodal distribution, indicating two photodissociation product channels. The slow component (II) is a broad peak at \sim 7 kcal/mol and

displays an isotropic distribution ($\beta \approx 0$), while the fast component (I) centers at ~ 50 kcal/mol and has an anisotropic angular distribution ($\beta \approx -0.23$). The fraction of the average translational energy release in the total available energy, $\langle f_{\rm T} \rangle$, is 0.13–0.17 for the slow pathway (II) and 0.62–0.72 for the fast pathway (I). The isotropic angular distribution and modest translational energy release for the slow component (II) suggest a statistical dissociation mechanism, leading to the formation of 1,3-butadiene + H on the ground electronic state after internal conversion from the excited Rydberg state. The high- $E_{\rm T}$, anisotropic component (I) is from a non-statistical dissociation process, occurring directly on an excited electronic state or a repulsive region of the ground electronic state which may involve a conical intersection, leading to the formation of 1,3-butadiene + H. The statistical unimolecular dissociation channel observed in this work is consistent with those previously reported in the studies of the 1-MA and 2-MA radicals. $^{9,12,34-35}$ The non-statistical photodissociation dynamics of the 1-MA radical is reported here for the first time.

Acknowledgements

This work was financially supported by the US National Science Foundation (No. CHE-2155232). Yuan Qin acknowledges support from a UC Riverside Dissertation-Year Fellowship. The REMPI spectra of 1-MA reproduced Figure 4(b) is from *Resonance Ionization Spectroscopy and Its Applications*, Institute of Physics Conference Series No. 94, edited by the Institute of Physics, Bristol, UK, Copyright © 1989 by Institute of Physics, pages 129-132. The specific content used includes Figure 2, which depicts the REMPI spectra of *cis*-1-methylallyl and *trans*-1-methylallyl between 455-485 nm, from the chapter titled "Resonance Enhanced Multiphoton Ionization Spectroscopy of 2-Butene-1-yl (C₄H₇) between 455-485 nm" by B. P. Tsai, R. D. Johnson III, and J. W. Hudgens.

Declaration of Conflicting Interests Statement

The Authors declare no competing financial interest.

Supporting Information

Additional computational details, including the structures, energies of excited states, transition dipole moments, and the NTO analysis of 1-MA calculated at different level of theories; calculation of the product translational energy distribution $P(E_T)$'s in the unimolecular dissociation of *trans*-1-MA to 1,3-butadiene + H using three statistical prior distribution models; and simulation of the signal decay in the H-atom pump-probe time profile.

References

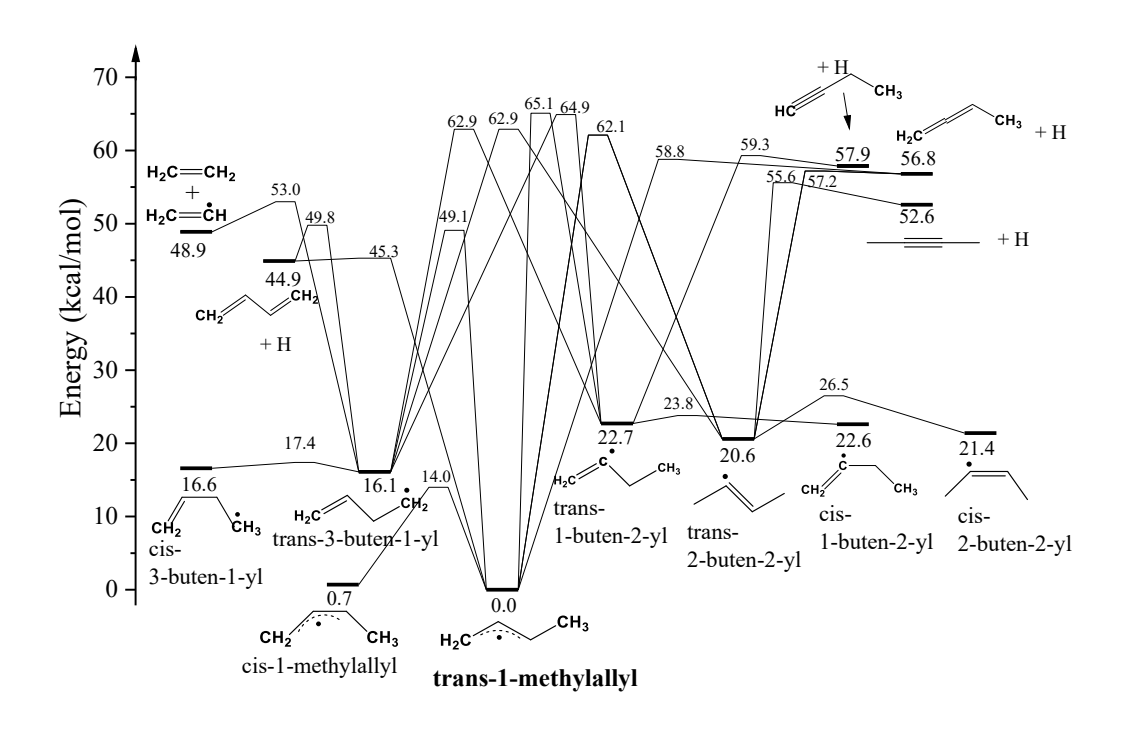
- 1. Callear, A.; Lee, H., Electronic spectra of the free allyl radical and some of its simple derivatives. *Trans. Faraday Soc.* **1968**, *64*, 308-316.
- 2. Kochi, J. K.; Krusic, P. J., Isomerization and electron spin resonance of allylic radicals. *J. Am. Chem. Soc.* **1968**, *90*, 7157-7159.
- 3. Brown, A. R.; Franke, P. R.; Douberly, G. E., Helium nanodroplet isolation of the cyclobutyl, 1-methylallyl, and allylcarbinyl radicals: Infrared spectroscopy and ab initio computations. *J. Phys. Chem. A* **2017**, *121*, 7576-7587.
- 4. Bahou, M.; Wu, J.-Y.; Tanaka, K.; Lee, Y.-P., Infrared absorption of *trans*-1-chloromethylallyl and *trans*-1-methylallyl radicals produced in photochemical reactions of *trans*-1, 3-butadiene and Cℓ₂ in solid *para*-hydrogen. *J. Chem. Phys.* **2012**, *137*, 084310.
- 5. Lang, M.; Holzmeier, F.; Hemberger, P.; Fischer, I., Threshold photoelectron spectra of combustion relevant C₄H₅ and C₄H₇ isomers. *J. Phys. Chem. A* **2015**, *119*, 3995-4000.
- 6. Schultz, J. C.; Houle, F.; Beauchamp, J., Photoelectron spectroscopy of isomeric C₄H₇ radicals. Implications for the thermochemistry and structures of the radicals and their corresponding carbonium ions. *J. Am. Chem. Soc.* **1984**, *106*, 7336-7347.
- 7. Röder, A.; Petersen, J.; Issler, K.; Fischer, I.; Mitric, R.; Poisson, L., Exploring the excited-state dynamics of hydrocarbon radicals, biradicals, and carbenes using time-resolved photoelectron spectroscopy and field-induced surface hopping simulations. *J. Phys. Chem. A* **2019**, *123*, 10643-10662.
- 8. B. P. Tsai; III, R. D. J.; Hudgens, J. W., Resonance enhanced multiphoton ionization spectroscopy of 2-butene-1-yl (C₄H₇) between 455-485 nm. In *Resonance Ionization Spectroscopy and Its Applications*, Institute of Physics: Bristol, UK, 1989; p 129.

- 9. Gasser, M.; Frey, J. A.; Hostettler, J. M.; Bach, A., Probing for non-statistical effects in dissociation of the 1-methylallyl radical. *Chem. Commun.* **2011**, *47*, 301-303.
- 10. Tarrant, D. H.; Getty, J. D.; Liu, X.; Kelly, P. B., Resonance Raman spectroscopy of the 1-methylallyl radical. *J. Phys. Chem.* **1996**, *100*, 7772-7777.
- 11. Miller, J. L., Theoretical study of the straight-chain C₄H₇ radical isomers and their dissociation and isomerization transition states. *J. Phys. Chem. A* **2004**, *108*, 2268-2277.
- 12. Gasser, M.; Bach, A.; Chen, P., Photodissociation dynamics of the 2-methylallyl radical. *Phys. Chem. Chem. Phys.* **2008**, *10*, 1133-1138.
- 13. Li, Y.; Liu, H.; Zhou, Z.; Huang, X.; Sun, C., Reaction mechanism of CH + C₃H₆: A theoretical study. *J. Phys. Chem. A* **2010**, *114*, 9496-9506.
- 14. Ribeiro, J. M.; Mebel, A. M., Reaction mechanism and product branching ratios of the CH + C₃H₆ reaction: A theoretical study. *J. Phys. Chem. A* **2016**, *120*, 1800-1812.
- 15. Li, Y.; Klippenstein, S. J.; Zhou, C.-W.; Curran, H., Theoretical kinetics analysis for H atom addition to 1, 3-butadiene and related reactions on the C₄H₇ potential energy surface. *J. Phys. Chem. A* **2017**, *121*, 7433-7445.
- 16. Huang, C.; Yang, B.; Zhang, F., Pressure-dependent kinetics on the C₄H₇ potential energy surface and its effect on combustion model predictions. *Combust. Flame* **2017**, *181*, 100-109.
- 17. Cho, J.; Jasper, A. W.; Georgievskii, Y.; Klippenstein, S. J.; Sivaramakrishnan, R., The role of energy transfer and competing bimolecular reactions in characterizing the unimolecular dissociations of allylic radicals. *Combust. Flame* **2022**, *257*, 112502.
- 18. Song, Y.; Lucas, M.; Alcaraz, M.; Zhang, J.; Brazier, C., Ultraviolet photodissociation dynamics of the phenyl radical. *J. Chem. Phys.* **2012**, *136*, 044308.

- 19. Amaral, G.; Xu, K.; Zhang, J., UV photodissociation dynamics of ethyl radical via the \tilde{A}^2 A' (3s) state. J. Chem. Phys. **2001**, 114, 5164-5169.
- 20. Xu, K.; Amaral, G.; Zhang, J., Photodissociation dynamics of ethanol at 193.3 nm: The Hatom channel and ethoxy vibrational distribution. *J. Chem. Phys.* **1999**, *111*, 6271-6282.
- 21. Song, Y.; Zheng, X.; Lucas, M.; Zhang, J., Ultraviolet photodissociation dynamics of the benzyl radical. *Phys. Chem. Chem. Phys.* **2011**, *13*, 8296-8305.
- 22. Woon, D. E.; Dunning Jr, T. H., Gaussian basis sets for use in correlated molecular calculations. IV. Calculation of static electrical response properties. *J. Chem. Phys.* **1994**, *100*, 2975-2988.
- 23. Martin, R. L., Natural transition orbitals. *J. Chem. Phys.* **2003**, *118*, 4775-4777.
- 24. Lucas, M.; Minor, J.; Zhang, J.; Brazier, C., Ultraviolet photodissociation dynamics of the *o*-pyridyl radical. *J. Phys. Chem. A* **2013**, *117*, 12138-12145.
- 25. Song, Y.; Lucas, M.; Alcaraz, M.; Zhang, J.; Brazier, C., Ultraviolet photodissociation dynamics of the allyl radical via the $\tilde{B}^2A_1(3s)$, $\tilde{C}^2B_2(3p_y)$, and $\tilde{E}^2B_1(3p_x)$ electronic excited states. J. Phys. Chem. A **2015**, 119, 12318-12328.
- 26. Lau, K.-C.; Liu, Y.; Butler, L. J., Photodissociation of 1-bromo-2-butene, 4-bromo-1-butene, and cyclopropylmethyl bromide at 234 nm studied using velocity map imaging. *J. Chem. Phys.* **2006**, *125*, 144312.
- 27. Reza, M. A.; Telfah, H.; Xu, R.; Liu, J., Room-temperature cavity ring-down spectroscopy of methylallyl peroxy radicals. *J. Phys. Chem. A* **2019**, *123*, 3510-3517.
- 28. Deyerl, H.-J.; Fischer, I.; Chen, P., Photodissociation dynamics of the allyl radical. *J. Chem. Phys.* **1999**, *110*, 1450-1462.

- 29. Castiglioni, L.; Bach, A.; Chen, P., Spectroscopy and dynamics of *A* [²B₁] allyl radical. *Phys. Chem. Chem. Phys.* **2006**, *8*, 2591-2598.
- 30. Glowacki, D. R.; Liang, C.-H.; Morley, C.; Pilling, M. J.; Robertson, S. H., MESMER: an open-source master equation solver for multi-energy well reactions. *J. Phys. Chem. A* **2012**, *116*, 9545-9560.
- 31. Pfeifle, M.; Ma, Y.-T.; Jasper, A. W.; Harding, L. B.; Hase, W. L.; Klippenstein, S. J., Nascent energy distribution of the Criegee intermediate CH₂OO from direct dynamics calculations of primary ozonide dissociation. *J. Chem. Phys.* **2018**, *148*, 174306.
- 32. Zare, R. N., Photoejection dynamics. *Mol. Photochem* **1972**, *4*, 1-37.
- 33. Yang, S. c.; Bersohn, R., Theory of the angular distribution of molecular photofragments. *J. Chem. Phys.* **1974**, *61*, 4400-4407.
- 34. Lucas, M.; Qin, Y.; Chen, M.; Sun, G.; Zhang, J., Ultraviolet Photodissociation of 2-Methylallyl Radical *Chin. J. Chem. Phys.* **2024**, *37*, 255-263.
- 35. Herterich, J.; Gerbich, T.; Fischer, I., Excited state dynamics of the 2-methylallyl radical. *ChemPhysChem* **2013**, *14*, 3906-3908.

Figures and captions



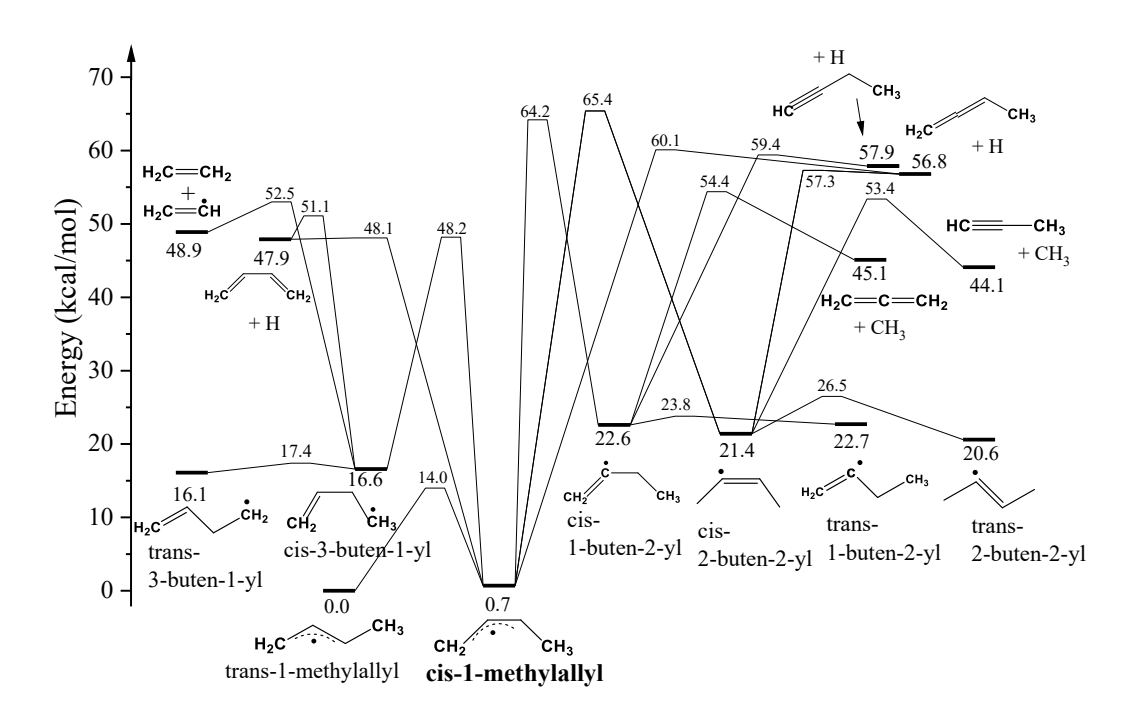


Figure 1. Potential energy diagram of C₄H₇ dissociation pathways relevant to this study. The energetics and pathways are based on the theoretical calculations in References 11-13.

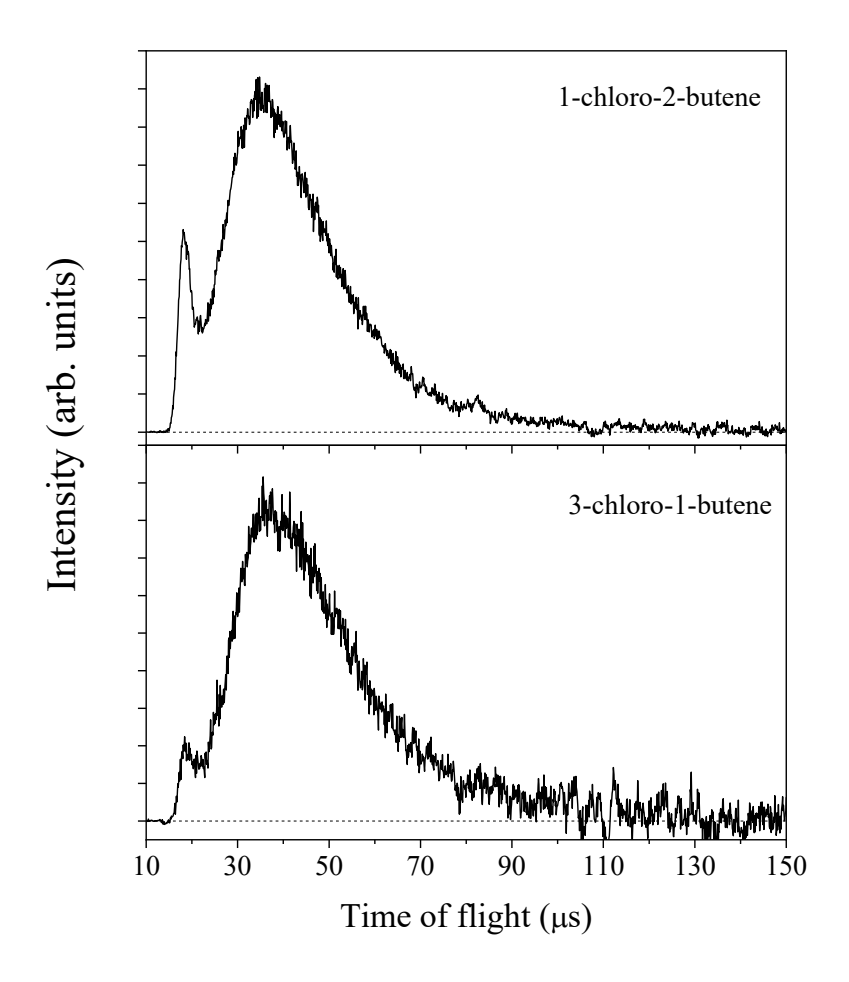


Figure 2. H-atom TOF spectra in the photodissociation of jet-cooled 1-methylallyl radical at 230 nm, produced from 193 nm photolysis of 1-chloro-2-butene (top) and 3-chloro-1-butene (bottom) precursors. These are the net H-atom TOF with the 193 nm photolysis radiation on minus off. The 230 nm radiation is polarized parallel to the TOF axis.

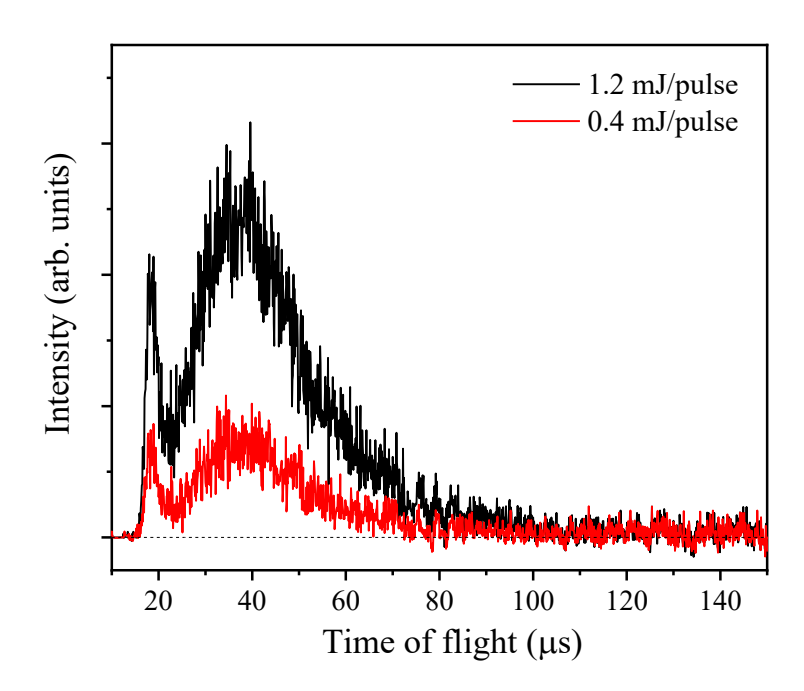


Figure 3. Photolysis laser power dependence: the H-atom product TOF spectra of the 1-methylallyl produced from the 1-chloro-2-butene precursor at 234 nm with photolysis energy 0.4 and 1.2 mJ/pulse. The TOF spectra are plotted on the same scale with the same number of laser shots. The signals have a linear dependence on the photolysis laser power.

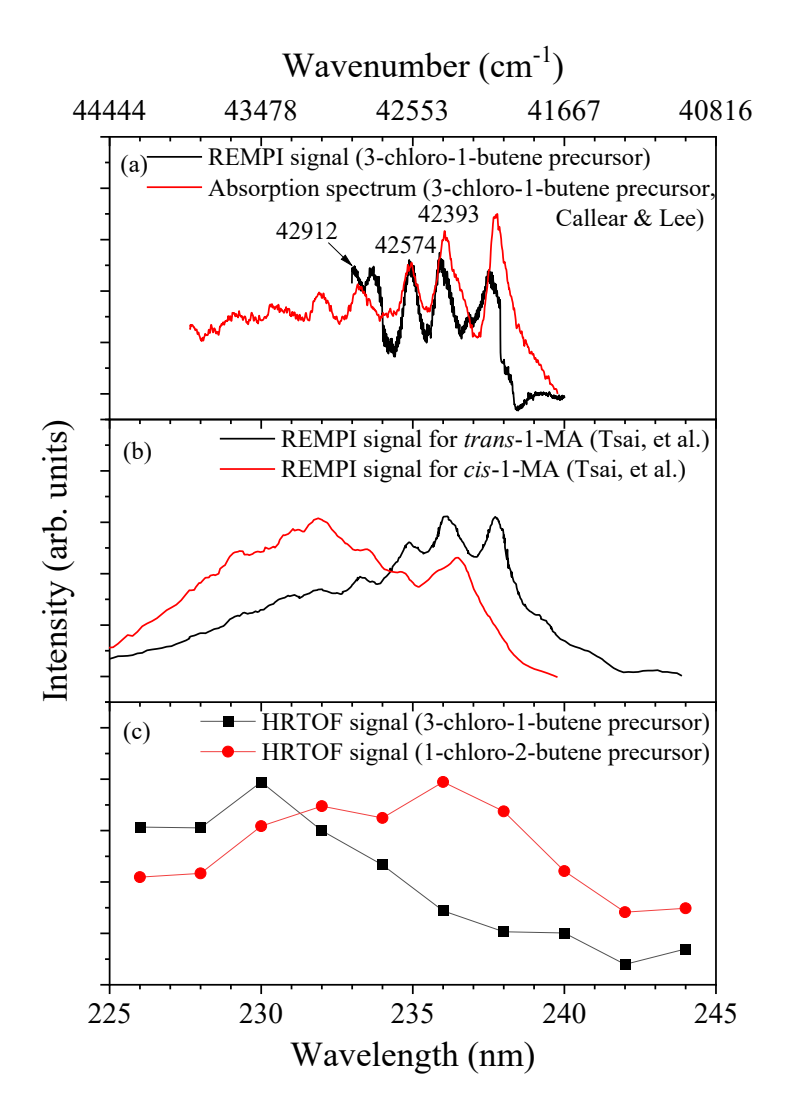


Figure 4. H-atom product yield (PFY) spectrum as a function of photolysis excitation energy in the region of 226–244 nm (the bottom panel (c)). The solid squares (■) represent the integrated HRTOF signals using 3-chloro-1-butene and the solid circles (●) represent the integrated HRTOF signals using 1-chloro-2-butene. The black line in the top panel (a) is the 1 + 1 REMPI spectrum of the 1-methylallyl radical generated from 3-chloro-1-butene in the region of 233–240 nm. The red line in the top panel (a) is the absorption spectrum (using 3-chloro-1-butene precursor) reproduced with permission from Ref. 1. The panel (b) shows the REMPI spectra of *trans*-1-MA and *cis*-1-MA taken from Ref. 8 (the excitation wavelength and energy are rescaled as the 2-photon excitation in 2 + 1 REMPI scheme).

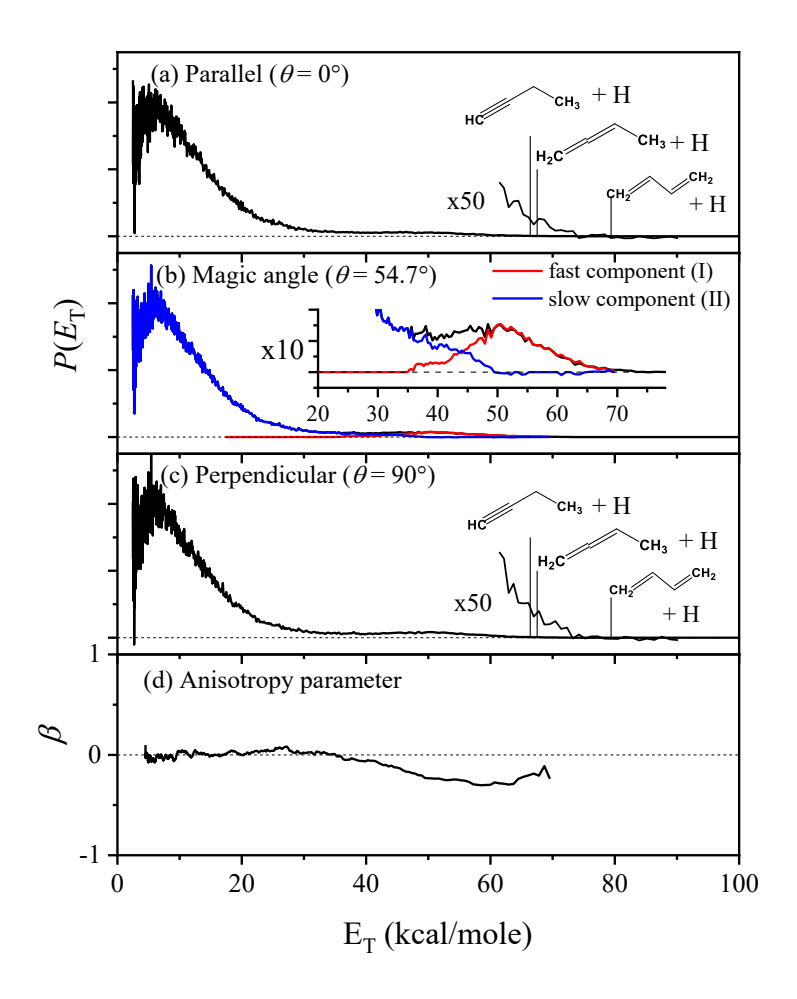


Figure 5. Center-of-mass product translational energy distribution, $P(E_T)$, of 1-methylallyl radical derived from the TOF spectra originating from the 1-chloro-2-butene precursor, with the 230 nm photolysis radiation polarization (a) parallel to the TOF axis, (b) at magic angle, and (c) perpendicular to the TOF axis. (d) Anisotropy parameter is derived from (a) and (c). $P(E_T)$ are plotted at the same scale. In (b), the magic-angle $P_m(E_T)$ distribution is de-convoluted with a fast component, $P_I(E_T)$ (red line) and a slow component, $P_{II}(E_T)$ (blue line). The vertical lines in (a) and (c) indicate the maximum translational energies of the H-atom product channels. See the text for details.

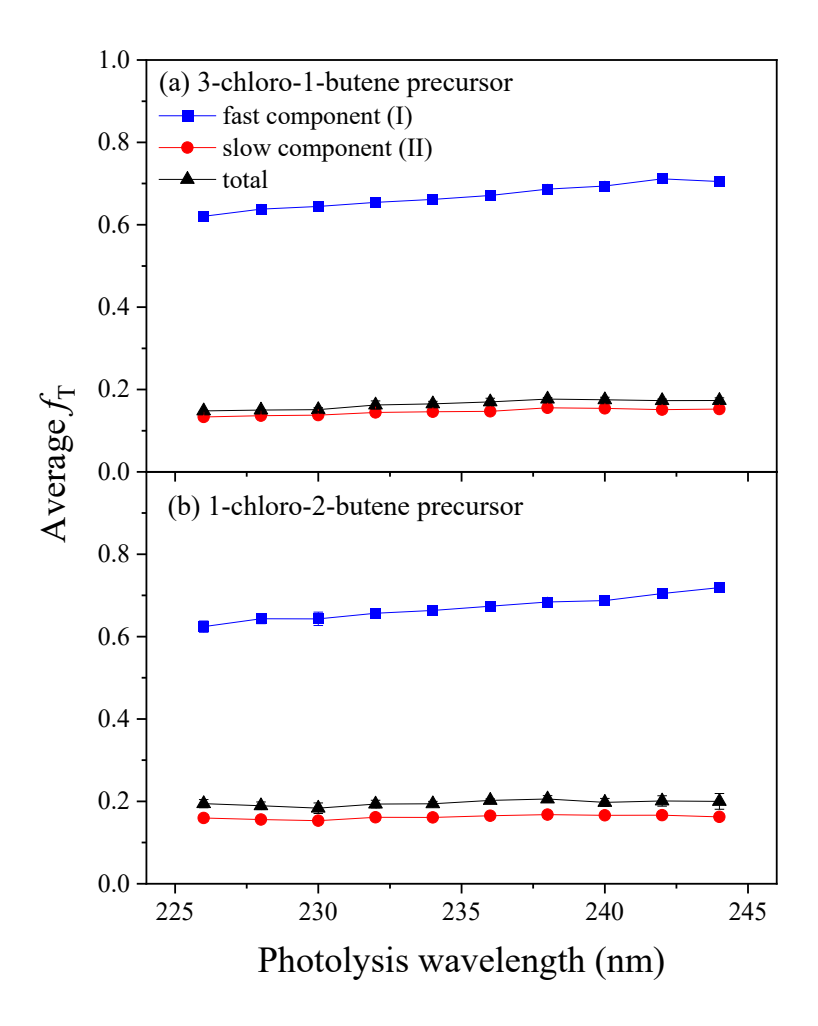


Figure 6. Photolysis wavelength and fraction of average translational energy release in the total available energy, $\langle f_{\rm T} \rangle$, in the UV photodissociation of the 1-methylallyl radical produced from two precursors. The average translational energies are calculated from the experimental $P(E_{\rm T})$ distributions. The total available energy at each photolysis wavelength is derived from the corresponding photon energy and the dissociation energy of 1-methylallyl to 1,3-butadiene + H for both the slow (red) and fast (blue) components. The error bars indicate the 95% confidence limit from multiple measurements.

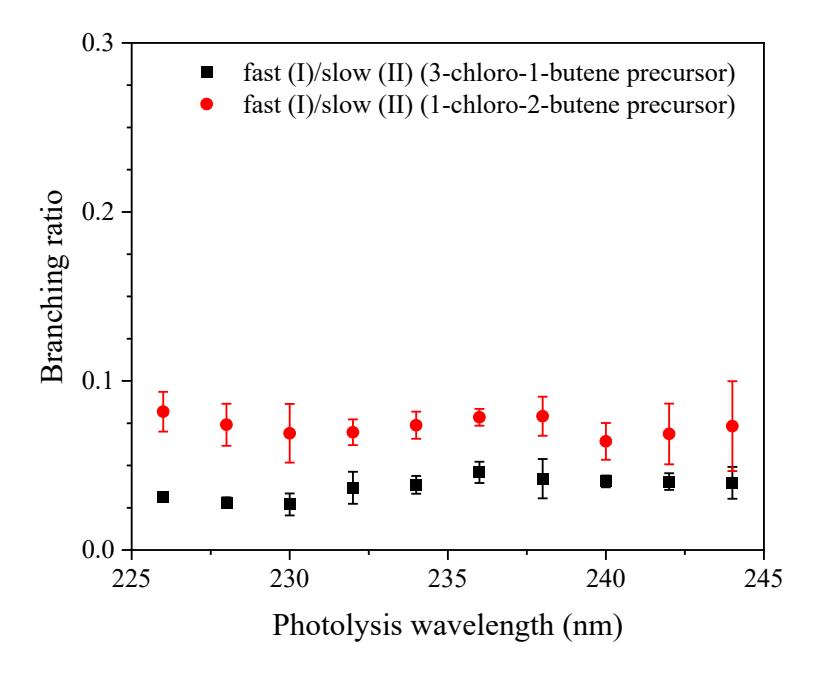


Figure 7. Photolysis wavelength and branching ratio of the fast and slow components in the UV photodissociation of the 1-methylallyl radical produced from two precursors. The intensities of the fast and slow components are obtained from integrating the deconvoluted fast and slow components in the fitted $P(E_T)$ distributions (for example, in Figure 5 for 230 nm). The error bars represent the 95% confidence limit from multiple measurements.

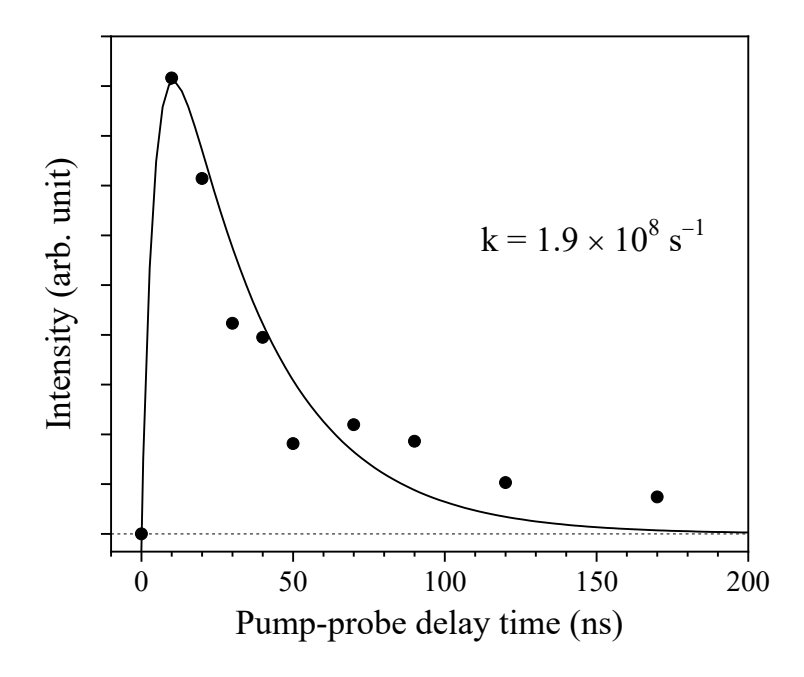


Figure 8. H-atom product signals from the 3-chloro-1-butene precursor as a function of photolysis and probe delay time at 230 nm. The signals (filled circles) are obtained by integrating the HRTOF spectra at the various photolysis-probe delay times. The line represents the exponential fit that gives the unimolecular decay rate constant.

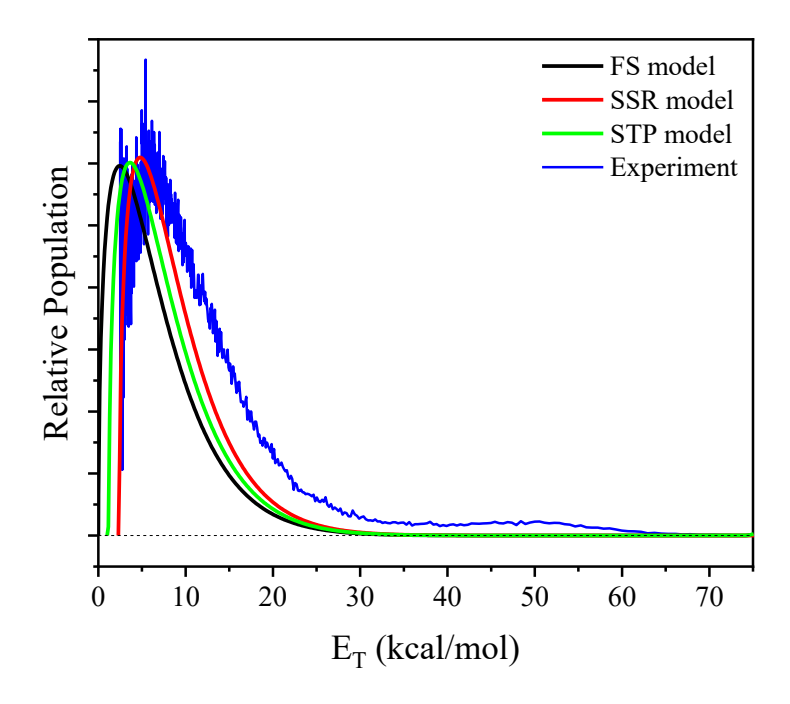


Figure 9. Comparison of the calculated and experimental product translational distribution $P(E_T)$ of 1-MA from the 1-chloro-2-butene precursor at 230 nm. The calculations from three statistical models assumed that *trans*-1-MA dissociates into 1,3-butadiene + H at 230 nm. In the STP model, 50 % of the energy of the exit channel barrier ($E_{TS} - E_{products}$) is assumed to channel into products' translation. See the text for details.